are based on subgroups of $P6_3/mmc$ result in very similar powder patterns. This applies in particular to the disorder types in Fig. 6.

The authors are indebted to the Deutsche Forschungsgemeinschaft and the Heinrich-Hertz-Stiftung for support of this work. Second-harmonic-generator investigations by T. Cline and W. Schulze (Pennsylvania State University) and electron-microscopic studies by Dr Köster (Ruhr University, Bochum) are gratefully acknowledged.

References

ARNOLD, H., KURTZ, W., RICHTER-ZINNIUS, A., BETHKE, J. & HEGER, G. (1981). *Acta Cryst.* B**37**, 1643-1651.
BELLANCA, A. (1942). *Period. Mineral.* **13**, 21-86.
BELLANCA, A. & CARAPEZZA, M. (1951). *Period. Mineral.* **20**, 271-307.
BERG, A. J. VAN DEN & TUINSTRA, F. (1978). *Acta Cryst.* B**34**, 3177-3181.
BOL'SHAKOV, K. A. & FEDOROV, P. I. (1956). *J. Gen. Chem. USSR*, **26**, 348-350.
BOL'SHAKOV, K. A., FEDOROV, P. I. & ILINA, N. I. (1963). *Russ. J. Inorg. Chem.* **8**, 1350-1352.
BREDIG, M. A. (1943). *J. Phys. Chem.* **47**, 587-590.
CALCAGNI, G. (1912). *Gazz. Chim. Ital.* **42**, 652-660.
CALCAGNI, G. & MAROTTA, D. (1912). *Gazz. Chim. Ital.* **42**, 674-686.
CALCAGNI, G. & MAROTTA, D. (1913). *Atti R. Accad. Naz. Lincei Mem. Cl. Sci. Fis. Mat. Nat. Sez.* II, **22**, 377.
CALCAGNI, G. & MAROTTA, D. (1915). *Gazz. Chim. Ital.* **45**, 368-376.
EVSEEVA, N. N. (1953). *Izv. Sekt Fiz.-Khim. Anal. Inst. Obshch. Neorg. Khim. Akad. Nauk. SSSR*, **22**, 162-169.
EYSEL, W. (1973). *Am. Mineral.* **58**, 736-747.
EYSEL, W. & HAHN, TH. (1970). *Z. Kristallogr.* **131**, 322-341.
FISCHMEISTER, H. (1962). *Monatsh. Chem.* **93**, 420-434.
GINSBERG, A. S. (1909). *Z. Anorg. Chem.* **61**, 126.
HÖFER, H. H. (1979). *Ionic Conductivity and Crystal Chemistry of* Na_2SO_4(I) *Solid Solutions with Aliovalent Cation Substitution* (in German). PhD Thesis, Technische Hochschule Aachen, Federal Republic of Germany.
HÖFER, H. H., VON ALPEN, U. & EYSEL, W. (1978). *Acta Cryst.* A**31**, S358.
HÖFER, H. H., EYSEL, W. & VON ALPEN, U. (1981). *J. Solid State Chem.* **36**, 365-370.
International Tables for X-ray Crystallography (1974). Vol. IV. Section 2.2. Birmingham: Kynoch Press.
IWAI, S., SAKAI, K. & WATANABE, T. (1973). *Kotai Butsuri*, **8**, 43-48.
KEESTER, K. L., EYSEL, W. & HAHN, TH. (1975). *Acta Cryst.* A**31**, S79.
KOBAYASHI, K. & SAITO, Y. (1982). *Thermochim. Acta*, **53**, 299-307.
MEHROTRA, B. N. (1973). *Structures and Phase Relations of Alkali Sulfates, Selanates, Chromates and Carbonates* (in German). PhD Thesis, Technische Hochschule Aachen, Federal Republic of Germany.
MEHROTRA, B. N., HAHN, TH., EYSEL, W. & ARNOLD, H. (1984). In preparation.
MIYAKE, M., MORIKAWA, H. & IWAI, S. (1980). *Acta Cryst.* B**36**, 532-536.
MÜLLER, H. (1910). *Neues Jahrb. Mineral. Geol. Palaeontol.* **30**, 1-54.
PERRIER, C. & BELLANCA, A. (1940). *Period. Mineral.* **11**, 163-300.
SCHUBERT, H. & EYSEL, W. (1980). *Proceedings of the Sixth International Conference on Thermal Analysis*, pp. 93-98. Basel: Birkhäuser.
STEWART, J. M., KRUGER, G. J., AMMON, H. L., DICKINSON, C. W. & HALL, S. R. (1972). The *XRAY*72 system-version of June 1972. Tech. Rep. TR-192. Computer Science Center, Univ. of Maryland, College Park, Maryland.

Acta Cryst. (1985). B**41**, 11-21

Investigation of Superlattices in K_xWO_3 in Relation to Electric Transport Properties

BY H. BRIGITTE KRAUSE

Physics Department, Northern Illinois University, DeKalb, IL 60115, *USA*

AND WILLIAM G. MOULTON AND R. C. MORRIS

Physics Department, Florida State University, Tallahassee, FL 32306, *USA*

(*Received* 23 *June* 1983; *accepted* 9 *August* 1984)

Abstract

Single crystals of K_xWO_3 were investigated with electron microscopy and X-ray diffraction methods. In most cases deviations from the hexagonal tungsten bronze structure in terms of commensurate and apparently incommensurate superlattices were observed. The commensurate superlattices in the a-b plane of the hexagonal lattice were, for most compounds, relatively simple, resulting in either an orthohexagonal unit cell or a hexagonal unit cell with two or four times the volume of the tungsten bronze structure, respectively. The 'incommensurate' superlattice rows in the **c** direction indicated a periodicity of 50 to 250 Å or more, depending in part on the crystal composition and temperature. Several different superlattice phases were observed. The superlattice formation is believed to be caused by ordering of the potassium atoms within the channels of the tungsten bronze structure. The data are consistent

0108-7681/85/010011-11$01.50

with the assumption of antiphase domains of a length of $4N+2$ layers with the integer N ranging from 3 to 16 or more. The length of these antiphase domains can vary within different parts of a single crystal and change with temperature owing to vacancy migration. The apparently incommensurate character of the superlattices may be caused by superposition of domains with different N values. Models of these antiphase domains for $x > 0{\cdot}25$ and $x < 0{\cdot}25$ are discussed. Diffraction patterns of Rb_xWO_3 showed only reflections of the regular tungsten bronze structure.

Introduction

The tungsten bronzes, compounds of composition M_xWO_3, where M is any of about 40 metallic elements and $0 < x < 1$, form a class of non-stoichiometric materials which crystallize in a number of different phases, and many have been found to have interesting properties. The cubic phases, and notably Na_xWO_3, have been studied extensively, while considerably less attention has been paid to the hexagonal phase until fairly recently. One group of hexagonal tungsten bronzes form when M = K, Rb or Cs for $0{\cdot}2 < x < 0{\cdot}33$. The crystal structure in the plane perpendicular to the c axis is shown in Fig. 1 (Magnéli, 1953). The work on hexagonal phases has revealed anomalies in the normal transport properties as a function of temperature; specifically, the resistivity, Hall coefficient and Seebeck coefficient (Stanley, Morris & Moulton, 1978, 1979; Skokan, Moulton & Morris, 1979; Caldwell, Morris & Moulton, 1981). These properties are a strong function of composition. The resistivity as a function of temperature (going from higher temperatures toward lower temperatures) shows a kink with onset at a temperature referred to as T_B. The Hall coefficient is constant above T_B and increases linearly with temperature below T_B, while the Seebeck coefficient shows a change of slope near T_B. The dependence of T_B on x shows a maximum at $x = 0{\cdot}25$ for both Rb_xWO_3 and K_xWO_3, as shown in Fig. 2. The Cs_xWO_3 shows no anomalies in the transport properties. In addition, the superconducting transition temperature, T_c, is a strong function of x, as shown in Fig. 3, while a smooth increase in T_c

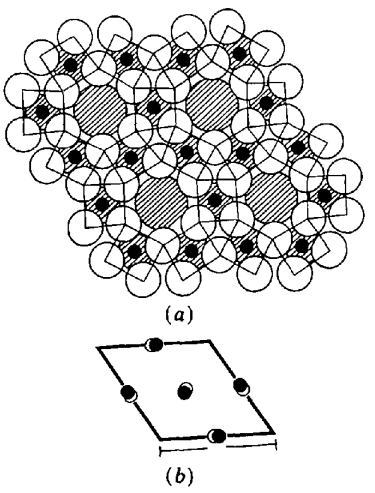

Fig. 1. Diagram of the M_xWO_3 hexagonal lattice showing the plane perpendicular to the c axis. The M ion sites reside in the holes formed by the WO_6 octahedra, and the structure is filled at $x = 0{\cdot}33$.

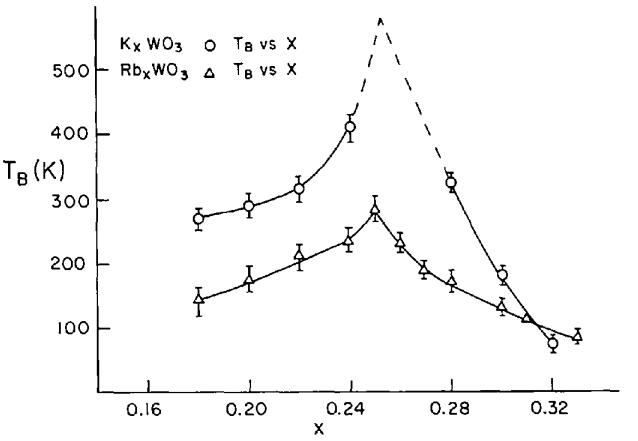

Fig. 2. Dependence of the onset temperature of the resistive anomaly, T_B, on composition in K_xWO_3 and Rb_xWO_3.

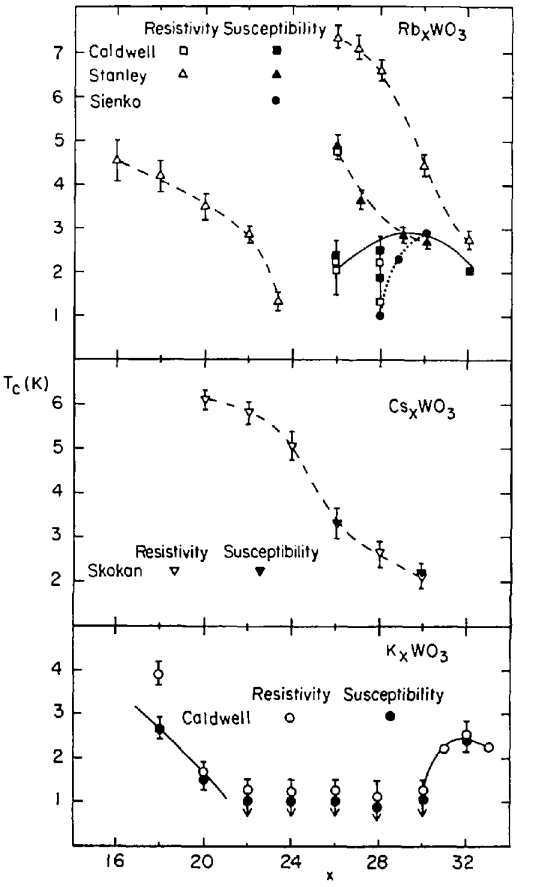

Fig. 3. Superconducting transition temperature, T_c, as a function of composition for K_xWO_3 and Rb_xWO_3.

is observed as x decreases in Cs_xWO_3. A strong 60° anisotropy in upper critical field Hc_2 is observed in the plane perpendicular to the c axis, as well as a 180° anisotropy perpendicular to the c axis for Rb_xWO_3 and Cs_xWO_3 at all reported values of x. It is currently accepted that the conduction band in all the tungsten bronzes is formed by donation of one electron from each metal insertion ion to the tungsten t_{2g} d orbitals, which interact with the oxygen $p\pi$ orbitals to form the band (Sienko, 1963; Goodenough, 1965; Ferretti, Rogers & Goodenough, 1965). If this model is correct the properties of the metal ion, such as size, determine differences in the transport and superconducting properties for different metal ions and concentrations. Qualitative models involving charge density waves, phase changes involving symmetry changes that cause a rapidly changing density of states or a possible ordering of the metal ions in the channels have been proposed. Which, if any, of these proposed models is correct can only be answered by careful structural studies of these systems. None of the earlier studies have shown any evidence of the structural changes proposed. A recent neutron diffraction study of Rb_xWO_3 powder

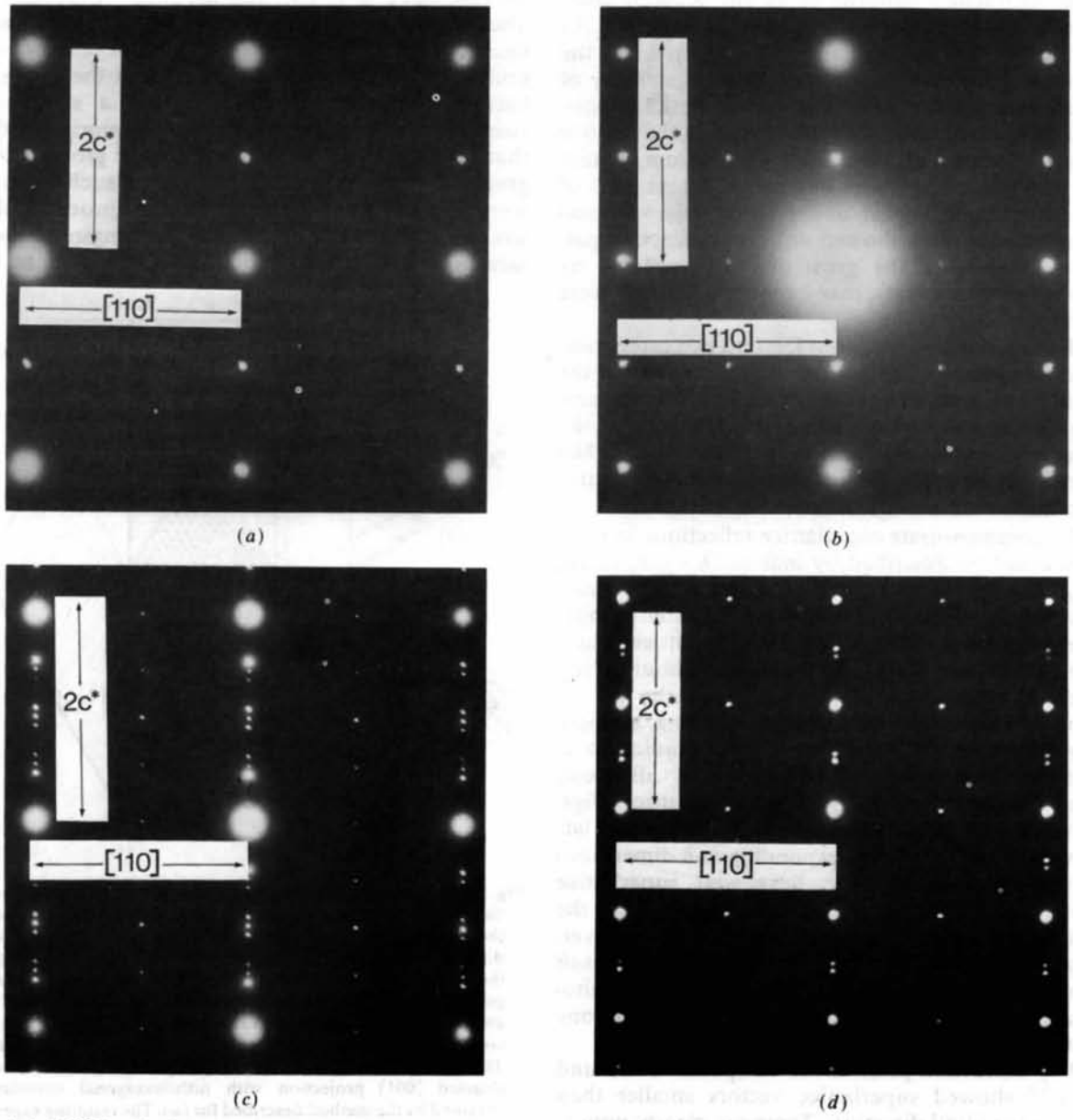

Fig. 4. (*a*) [1$\bar{1}$0] projection of $K_{0\cdot33}WO_3$ showing no superlattice reflections. (*b*) [1$\bar{1}$0] projection of $K_{0\cdot24}WO_3$ showing commensurate superlattice reflections only. (*c*) [1$\bar{1}$0] projection of $K_{0\cdot22}WO_3$ showing both commensurate and incommensurate superlattice reflections. (*d*) [1$\bar{1}$0] projection of $K_{0\cdot26}WO_3$ showing both commensurate and incommensurate superlattice reflections.

samples showed evidence of ordering of the Rb atoms below T_B (Sato, Grier, Shirane & Fujishita, 1982). Bando & Iijima (1980) found incommensurate superlattice reflections for $K_{0.30}WO_3$. In the present work a careful electron and X-ray study of single crystals of the K_xWO_3 systems was carried out in order to explore more fully the validity of the proposed models.

Results

A. *HVEM† room-temperature data*

The diffraction patterns of all the K_xWO_3 compounds contained the reflections to be expected for a tungsten bronze structure as reported in the literature. However, in addition, a great number of superlattice reflections were observed. Both the positions of these superlattice reflections and the relative intensities varied with the relative potassium content and with the temperature. But even different parts of the same single crystal under apparently identical circumstances often showed different diffraction patterns. In spite of the great diversity revealed by detailed measurements, many common features were found.

The superlattice reflections fell into two categories: (1) commensurate superlattice reflections within the a^*-b^* planes; and (2) closely spaced incommensurate reflections along rows perpendicular to the a^*-b^* plane and originating from each of the regular $hk0$ reflections, or from the commensurate superlattice reflections.

The commensurate superlattice reflections in most cases could be described by indices $(h+\frac{1}{2}, k, l)$, $(h, k+\frac{1}{2}, l)$ or $(h+\frac{1}{2}, k+\frac{1}{2}, l)$ (Figs. 4 and 6). The direct observations of the [001] projection indicated in most cases hexagonal symmetry of the superlattice. But a reconstruction of the a^*-b^* plane from about twenty different projections perpendicular to the a^*-b^* plane - which were obtained by rotating a single crystal through 70° about the c axis - indicated at least in one case of $K_{0.25}WO_3$ a different, orthohexagonal, symmetry of the superlattice. Figs. 5(a) and 5(b) show the reconstructed reciprocal lattices and Fig. 5(c) the corresponding a-b dimensions of the superlattices. The hexagonal superlattice implies quadrupling of the unit-cell volume while the orthohexagonal cell implies only doubling. However, hexagonal superlattices (Fig. 5) could possibly result from the superposition of microtwinned orthohexagonal sections rotated by 60° relative to one another.

Only diffraction patterns for compositions around $x=0{\cdot}25$ showed superlattice vectors smaller than $a^*/2$ in the [100] direction. These are clearly noticeable in reciprocal-lattice layers with an odd l in Fig. 6(a). The diffuse reflections around $[h/4, 0, (2n+1)l]$ *etc.* consist of closely spaced reflections corresponding to more than 200 Å distances in real space. In addition to the disordered phase of Fig. 6(a) two ordered commensurate phases were found for $K_{0.25}WO_3$, one with doubling of all lattice constants, one with doubling of the a dimension, but quadrupling of the c dimension. The corresponding diffraction patterns are shown in Figs. 6(b) and 6(c).

The incommensurate reflections in the form $h,k,l+\Delta l$ occur in two groups: one centered around and containing the hkl reflections and the other centered around, but not containing, the $h,k,l+\frac{1}{2}$ reflections. The intensities of both groups are asymmetrically decreasing from the center towards both sides of each group. For a given diffraction pattern the intervals between adjacent reflections within a group are (within the error of measurement) identical provided that the reflections belong to the same group. For a great number of diffraction patterns all such intervals were measured and averaged. The reciprocal of that average in units of one layer of the tungsten bronze structure was called 'periodicity' and used as the

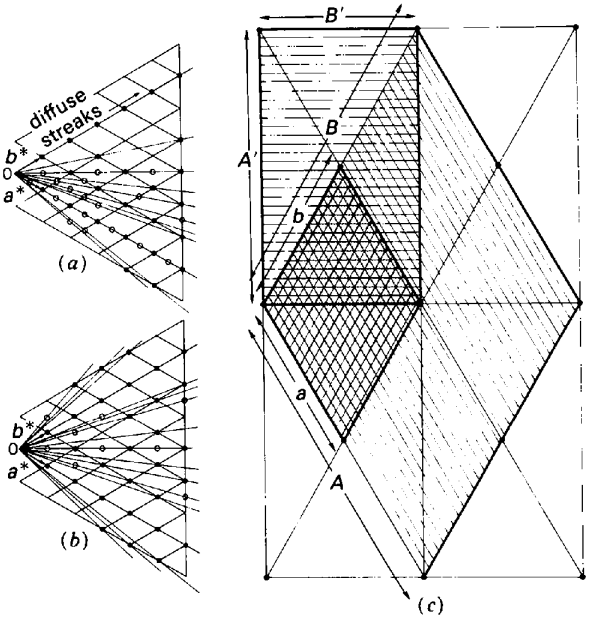

Fig. 5. (a) Reconstructed [001] projection with hexagonal superlattice. By containing the c axis of a crystallite perpendicular to the electron beam, and rotating the crystal about this zone axis, diffraction patterns of all major projections within the range of the tilting stage were taken. Thus, one $hk0$ vector for each projection was obtained. The combined information from different $[hk0]$ vectors was used to construct a model containing the commensurate superlattice reflections of the $[00l]$ projection. The resulting superlattice vectors are $\frac{1}{2}\mathbf{a}^*$ and $\frac{1}{2}\mathbf{b}^*$. (b) Reconstructed [001] projection with orthohexagonal superlattice obtained by the method described for (a). The resulting superlattice vectors are $\frac{1}{2}\mathbf{a}^*+\frac{1}{2}\mathbf{b}^*$ and $\frac{1}{2}\mathbf{a}^*-\frac{1}{2}\mathbf{b}^*$. ($c$) Relationship between tungsten bronze lattice dimensions and hexagonal and orthohexagonal superlattices.

† High-voltage electron microscope.

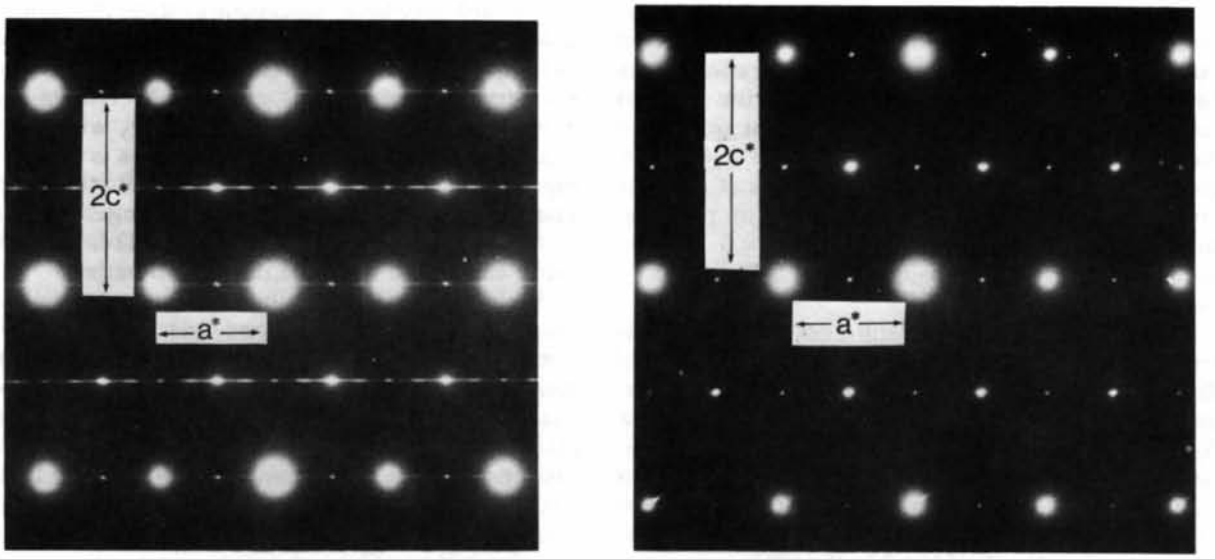

(*a*) (*b*)

Fig. 6. [120] projection of $K_{0.25}WO_3$. (*a*) Partially ordered with diffuse streaks. Superlattice reflections occur at $(2n+1)h/2,(2m+1)k/2,l$ positions (m, n = integers) and are most intense perpendicular to [00*l*] for odd l values. The diffuse streaks are also most pronounced for odd l values. (*b*) Ordered commensurate superlattice with lattice constants 2*a* and 2*c*.

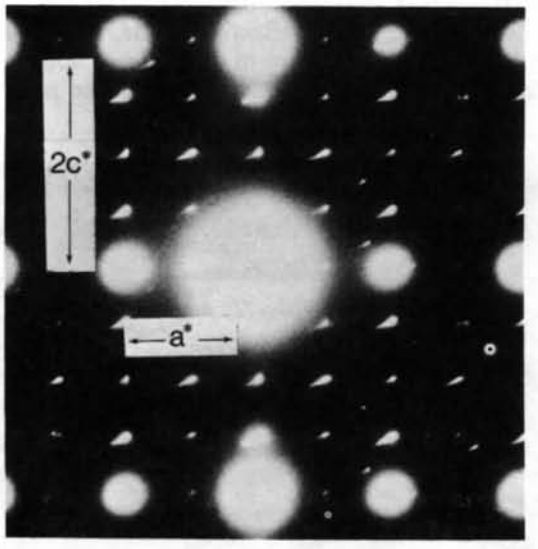

(*c*)

Fig. 6 (*cont.*) (*c*) Ordered commensurate superlattice with lattice constants 2*a* and 4*c*.

abscissa in Fig. 7. At this time the periodicity is simply a parameter; the physical meaning of it will be discussed later. The actual spacings of diffraction spots between $(h,k,2l)$ and $(h,k,2l+1)$ in reciprocal space are drawn along the z direction. Both $z=2l$ and $z=2l+1$ are mirror planes, and the intensities are more or less symmetrical with respect to these planes, but not with respect to $z=2l+\frac{1}{2}$ and $z=2l+\frac{3}{2}$. The positions of the diffraction spots, however, are also symmetrical with respect to $z=2l+\frac{1}{2}$ and $z=2l+\frac{3}{2}$, and, therefore, only the interval between $z=2l$ and $z=2l+1$ is shown. The composite data in Fig. 7 determine a family of curves which, for periodicities of the form $y=4N+2$, are evenly spaced. Thus the intersections of the curves with $y=4N+2$ define the positions of commensurate superlattice reflections for a superlattice with the periodicity $4N+2$ layers. The curves in Fig. 7 were actually calculated by interpolation between the commensurate superlattice reflections for $y=4N+2$ by connecting the reflections closest to $z=2l$, closest to $z=2l+\frac{1}{2}$, and $z=2l+1$, second closest to $z=2l$, $z=2l+\frac{1}{2}$ and $z=2l+1$, *etc.* The agreeement between the so calculated and observed values over the whole range of periodicities is excellent. It should be noted, however, that, except for $y=4N+2$, the spacing between the closest reflections of different groups is not an integral multiple of the interval between adjacent reflections of the same group and, therefore, the 'periodicity' cannot be interpreted in a straightforward fashion as the superlattice cell constant. It will be shown later that the 'periodicity' represents an average period resulting from the superposition of superlattices with different lattice constants of the form $4N+2$ layers in different domains of the crystal.

The only simple conclusion to be drawn from Fig. 7 is that almost all of the diffraction patterns, regardless of composition and temperature, can be represented by the family of curves shown in Fig. 7. A clear relationship between the layer periodicity and the potassium concentration of the sample could not be established although trends were observed. Around

$x = 0{\cdot}25$ the layer periodicity was highest, in some cases around sixty, seventy, or more. It decreased both towards higher and lower concentrations. It is believed that the sample composition for a given diffraction pattern was not exactly known and that it was not uniform within a crystallite. This was concluded from the fact that different parts of a single crystal sometimes gave different diffraction patterns. In particular, some samples marked as $x = 0{\cdot}24$ were, based on theoretical considerations, believed to be $x = 0{\cdot}25$.

The relative intensities of different diffraction patterns, however, vary sufficiently to assume several distinct crystal phases: for $x = 0{\cdot}25$ exactly three-quarters of the potassium positions are occupied. Around this composition the incommensurate superlattice reflections in the [00l] direction disappear. For $0{\cdot}25 < x < 0{\cdot}29$ strong incommensurate superlattice reflections are observed with the most intense of these reflections for $\Delta l = N/4N + 2$ in the [00l] reciprocal-lattice row. Around $x = 0{\cdot}29$ seven-eighths of the potassium positions are occupied and above that x value a different kind of ordering takes place. Below $x = 0{\cdot}25$ (for $x = 0{\cdot}22$) the two incommensurate superlattice reflections at $l = \pm N/4N + 2$ are almost equally strong and are the only observable superlattice reflections between $z = 2l$ and $2l + 1$. Thus, for both $x < 0{\cdot}25$ and $x > 0{\cdot}25$ most of the scattering power of the superlattice peaks is near $z = 2l + \frac{1}{2}$ (corresponding to a four-layer period in real space). For $x = 0{\cdot}25$ the scattering power occurred exactly at $z = 2l + 0{\cdot}25$. That corresponds with the asymptotic approximation for a period of infinity in Fig. 7.

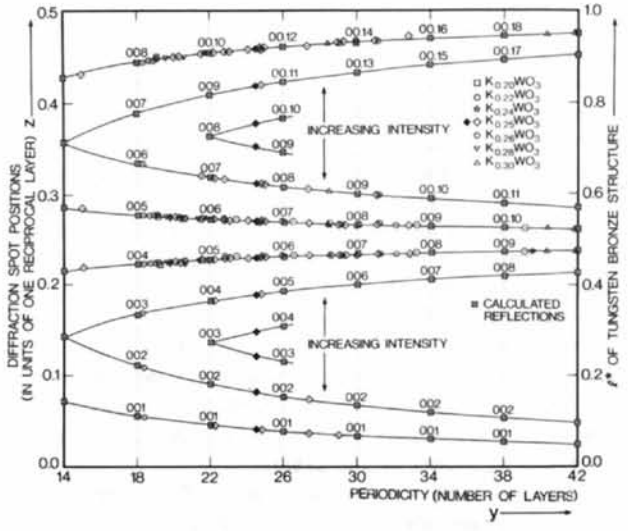

Fig. 7. Composite chart of incommensurate lattice reflections from crystals of different composition at different temperatures. Open symbols: observed data for low-temperature phases; filled symbol: high-temperature phase; ⊠: calculated reflections for periodicities of $4N + 2$; solid lines: calculated lines as explained in the text, compatible with simple diffraction.

It would have been interesting to study the complex ordering phenomena with high-resolution imaging techniques, but the small contrast at high voltages is not very suitable for this method. A medium-resolution image of a region of $K_{0{\cdot}26}WO_3$ with strong incommensurate superlattice reflections is shown in Fig. 8 which was taken with a JEOL 100 microscope. The distance between the prominent fringes is around 70 Å, corresponding roughly with the 22-layer periodicity calculated from the diffraction pattern.

While the incommensurate reflections were most pronounced for compositions that do not allow a simple ordering of the potassium atoms, the commensurate reflections were particularly developed near compositions where such ordering can take place: $x = 0{\cdot}25$, $x = 0{\cdot}29$ or $x = 0{\cdot}20$. In most of these cases both the a dimension of the hexagonal lattice and the c dimension were doubled. The superlattices often showed rather strong reflections of the form $h + \frac{1}{2}, k + \frac{1}{2}, 2l + 1$. The ordering in most cases was not complete, and diffuse scattering along lines or sheets perpendicular to c, especially for odd l values, was observed (Figs. 6a and 9a). Weaker diffuse sheets were also observed in the a–c planes (Fig. 10). In some cases each reflection showed a fine structure if viewed under a low-magnification microscope.

The intensities of the reflection of the regular tungsten bronze structure were in general not noticeably different in samples that yield superlattice patterns

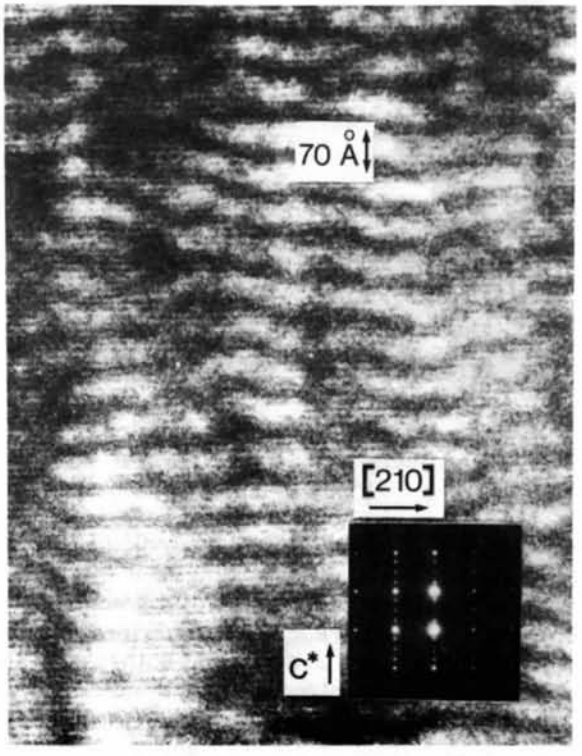

Fig. 8. Image of $K_{0{\cdot}26}WO_3$ showing lattice fringes.

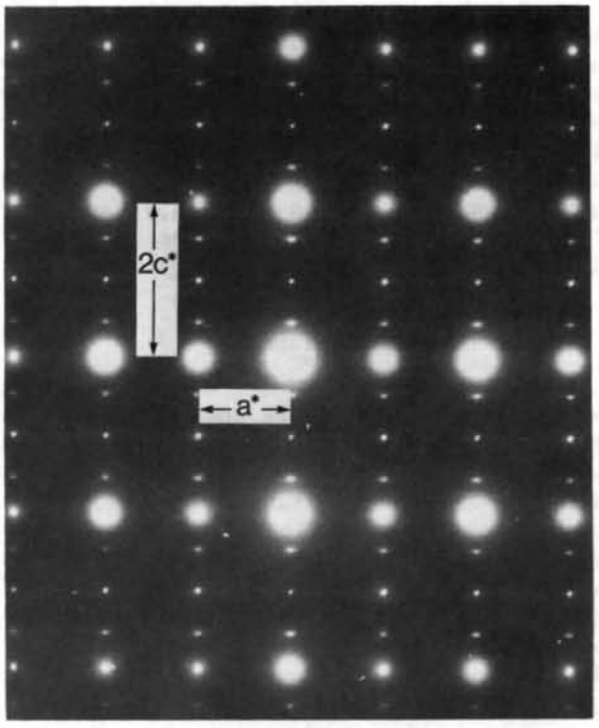

(*a*)

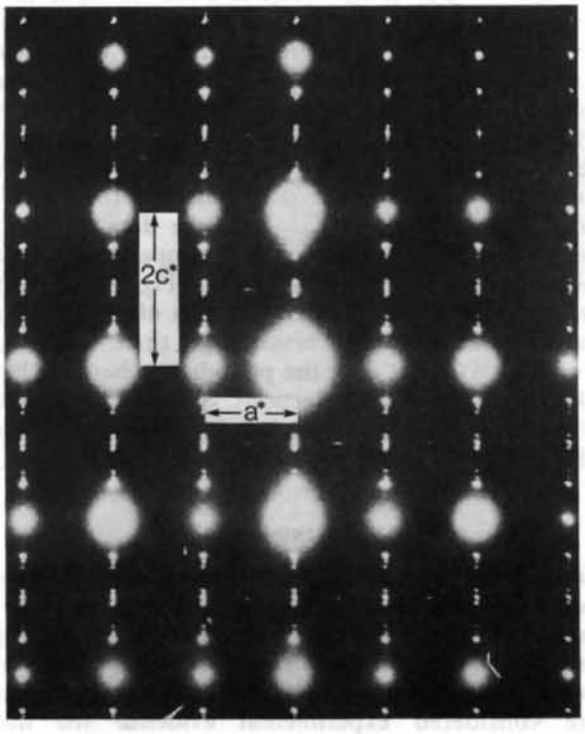

(*b*)

Fig. 9. (*a*) [1$\bar{2}$0] projection of disordered incommensurate superlattice of $K_{0.26}WO_3$. (*b*) Equivalent projection of the same crystal segment 60° apart showing a higher degree of order.

and those which did not. Exceptions were the reflections with odd l values, which sometimes changed their intensities relative to the reflections with an even l in the course of prolonged irradiation with electrons.

B. Room-temperature X-ray data

Weissenberg photographs were taken for $K_{0.22}WO_3$, $K_{0.25}WO_3$, $K_{0.28}WO_3$ and $K_{0.30}WO_3$. According to Magnéli (1953), conditions limiting possible reflections are: $h\bar{h}0l$, $l=2n$, in accordance with the space groups $P6_3/mcm$, $P\bar{6}c2$ or $P6_3cm$. While the $h\bar{h}0l$ reflections were almost completely absent for odd values of l, some very weak $h\bar{h}kl$ reflections were observed for $K_{0.28}WO_3$ and $K_{0.30}WO_3$ indicating that none of the proposed space groups is correct. Diffractometer measurements indicated that the odd $00l$ reflections are missing. A new structure determination of the tungsten bronze structure is being performed in cooperation with Argonne National Laboratory and will be published at a later date.

The lattice constants determined from the Weissenberg photographs – ignoring superlattice reflections – were: $a=7{\cdot}38$ and $c=7{\cdot}52$ Å. The c/a ratio of 1·02 corresponded with measurements from the electron diffraction patterns. The X-ray film methods were too inaccurate to determine possible small lattice-constant changes as a function of composition. Commensurate superlattice reflections within the a^*–b^*

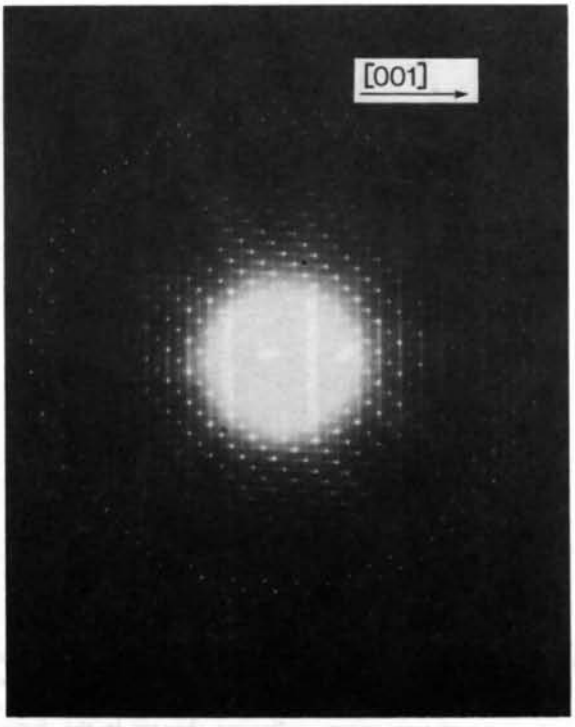

Fig. 10. Diffraction pattern showing strong diffuse features.

planes could not be detected, but layers of incommensurate reflections on both sides of the reciprocal halfway point between regular reciprocal a^*-b^* layers could be observed in rotation photographs of $K_{0.25}WO_3$, $K_{0.26}WO_3$, $K_{0.28}WO_3$ and $K_{0.30}WO_3$. In accordance with the electron diffraction data they were too weak to show up for $K_{0.22}WO_3$. Also absent were any incommensurate superlattice reflections in rotation photographs of $Rb_{0.25}WO_3$.

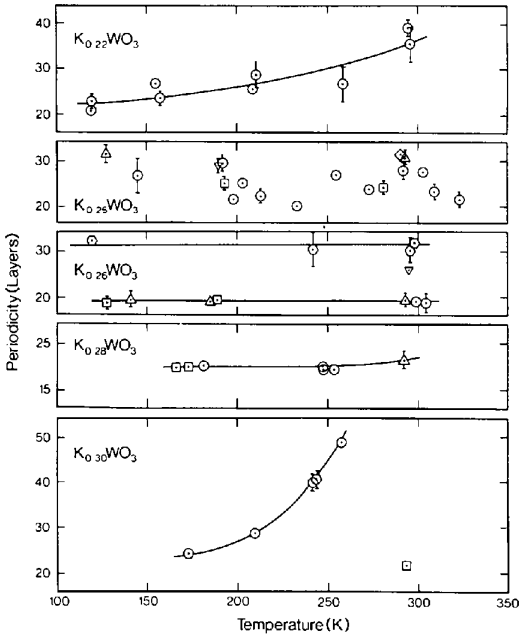

(*a*)

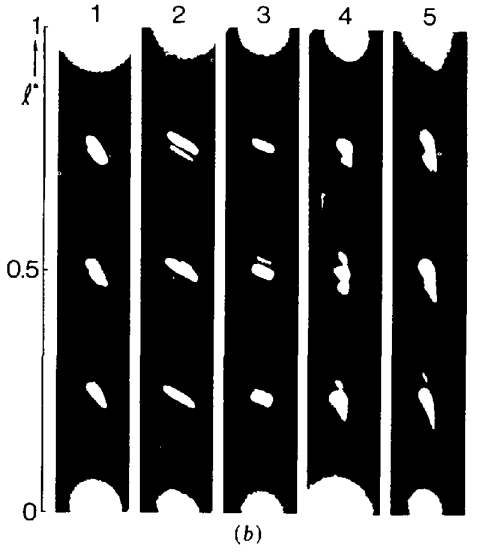

(*b*)

Fig. 11. (*a*) The temperature dependence of the incommensurate superlattice periodicity for $K_{0.22}WO_3$, $K_{0.25}WO_3$, $K_{0.26}WO_3$ and $K_{0.30}WO_3$. (*b*) Changes of the shape of $K_{0.30}WO_3$ reflections as a function of temperature indicating changes in the domain configuration.

Some initial line-profile measurements of high-order $h00$ reflections of $K_{0.25}WO_3$ and $K_{0.22}WO_3$ were taken on an X-ray single-crystal diffractometer. For one crystal of $K_{0.25}WO_3$ a small line splitting of the 800 reflection in all six equivalent crystallographic directions was observed. A reconstruction of the α_1-α_2 line profiles of the four resulting peaks yielded lattice constants of $a = 7{\cdot}3826\,(5)$ and $c = 7{\cdot}3886\,(2)$ Å, respectively. Another sample of $K_{0.25}WO_3$ did not show such splittings.

C. Temperature-dependent data

Thinned single crystals of $K_{0.25}WO_3$ and $K_{0.26}WO_3$ were exposed to temperatures ranging from 120 K to about 370 K. Each of the experimental runs extended over many hours or even over days. While attempts were made to examine the same crystal area at different temperatures, it was also realized that some radiation damage had taken place over extended periods of time. It was, for instance, noted that the ratio of intensities between incommensurate superlattice points and regular tungsten bronze reflections decreased regardless of whether the temperature was increased or decreased. In particular, the *hkl* reflections with odd *l* increased in relative intensity as the result of radiation. Because of the apparent radiation damage it was sometimes necessary to switch to another domain in the course of a run taking several days. It became evident only in retrospect that different domains behave differently and may even have different compositions. As a result there is a large amount of scattering in the observed data as is evident in Fig. 11. For $K_{0.26}WO_3$, for instance, the upper of the two curves obtained from one crystal segment is quite different from the data obtained from other crystal segments. For $K_{0.25}WO_3$ the data scattered widely. In one case above room temperature a new phase was observed for $K_{0.25}WO_3$ (Fig. 12). A very strong change with temperature was observed for x values much smaller or much larger than $K_{0.25}WO_3$. For $K_{0.30}WO_3$ not only the periodicity changed, but also the shape of the reflections, indicating an extensive reorganization of the whole domain structure (Fig. 12).

Discussion

Since all of the K_xWO_3 compounds for $x < 0{\cdot}33$ are potassium deficient, one may assume that the superlattice formation - at least in part - is caused by ordering of the potassium vacancies within the channels parallel to the **c** direction. The following points are considered experimental evidence for this assumption.

(1) The intensity pattern of the reflections (other than superlattice reflections) is similar in diffraction patterns containing superlattice spots and those not

showing any superlattice features. This holds true for all major projections investigated.

(2) The commensurate superlattice reflections in the a^*-b^* plane cannot readily be observed with X-rays. This can be explained by assuming that the commensurate superlattice reflections are caused by a different ordering of vacancies along symmetrically unrelated channels. Since the scattering power of potassium *vis-à-vis* that of tungsten is much smaller for X-rays than for electrons, the superlattice reflections do not show up in the X-ray data.

(3) The incommensurate superlattice reflections are strong for compositions with vacancy ratios that do not allow a simple ordering within a few unit cells. For $K_{0\cdot25}WO_3$, on the other hand, every fourth potassium position is vacant and, therefore, simple ordering is possible and is observed. For incommensurate vacancy-occupied position ratios the ordering requires large unit cells and the incommensurate reflections in rows parallel to **c** indicate a long period of the superlattice of up to several hundred ångströms. Such a long periodicity could easily result from ordering of vacancies. The vacancies here could cause slight changes in the layer distance of the tungsten bronze structure. As a result of these changes the superlattice reflections become strong enough to be noticeable in X-ray patterns.

(4) The apparently complex data in Fig. 7 can be explained by assuming vacancy ordering along the channels: the strong scattering near reciprocal-lattice points that represent a four-layer distance suggest vacancies at four-layer intervals. However, the observed reflections do not occur for $2l \pm \frac{1}{2}$, but symmetrically with respect to this reciprocal-lattice point. This observation and the fact that only for periodicities of $4N+2$ agreement between the expected and observed reflection positions exist suggest the presence of antiphase domains of period $4N+2$ layers. The antiphase domains can be coupled in different ways. Two of these arrangements, called models 1 and 2, result in compositions $x<0\cdot25$ and $x>0\cdot25$, respectively, and agree relatively well with the observed data. In model 1 chains of the form *V*KKK*V*KKK*V*KKK*V*... are coupled by only one K, while in model 2 the same sequence *V*KKK*V*KKK*V*... is linked by KKKK*V*KKKK (K stands for potassium, *V* for vacancy). The vacancies of the second domain thus are out of phase with the vacancies of the first domain and consequently the $l=2N\pm0\cdot5$ reciprocal-lattice points become antinodes rather than reflections although considerable scattering intensity is found in the proximity of these points. The diffraction patterns along [00*l*] (ignoring form factors, polarization *etc.*) obtained by simple calculations of a one-dimensional array of scatterers according to models 1 and 2 are shown in Figs. 13(*a*) and (*b*). The positions of the diffraction peaks are the same as for the observed superlattice reflections, and the intensities agree reasonably well with Figs. 4(*c*) and (*d*), respectively. Fig. 13(*c*) simulates the situation where the crystallite contains an equal number of ordered segments of different chain lengths

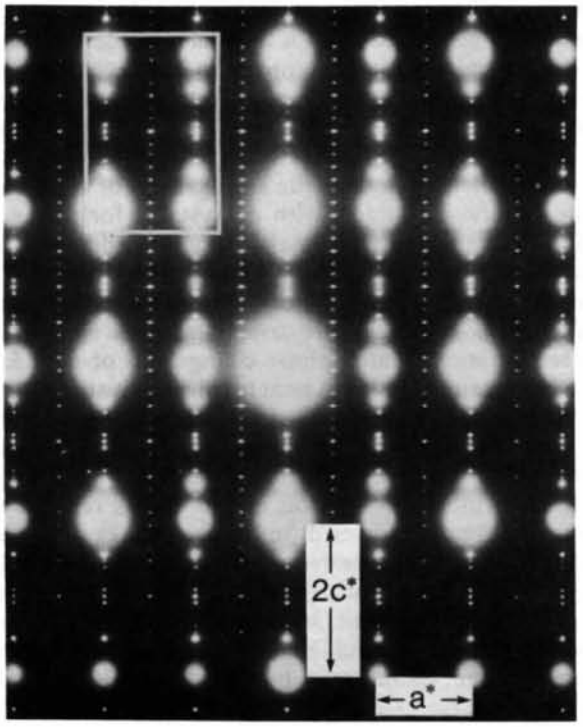

(*a*)

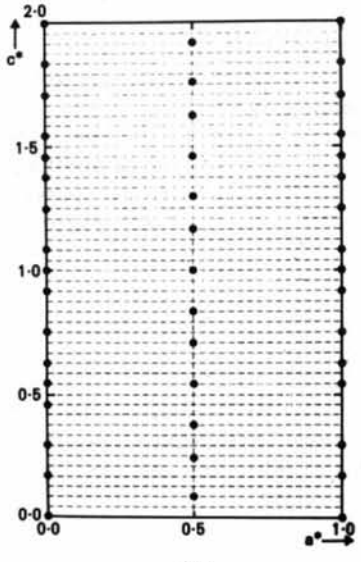

(*b*)

Fig. 12. High-temperature modification of $K_{0\cdot25}WO_3$. (*a*) Observed diffraction pattern. (*b*) Reconstructed part of the diffraction pattern. The superlattice would be commensurate with a 24-layer periodicity in the **c** direction if the reflections were exactly on the dotted line. A careful measurement of reflection positions shows small displacements from these lines. These follow the pattern of Fig. 7.

$4N+2$ and $4(N+1)+2$. The good agreement with the observed reflection patterns suggests from the data in Fig. 7 that 'periodicities' other than $4N+2$ result from superposition of data from crystal segments with $4N+2$ layer periods. The 'periodicity' then represents the average lattice constant.

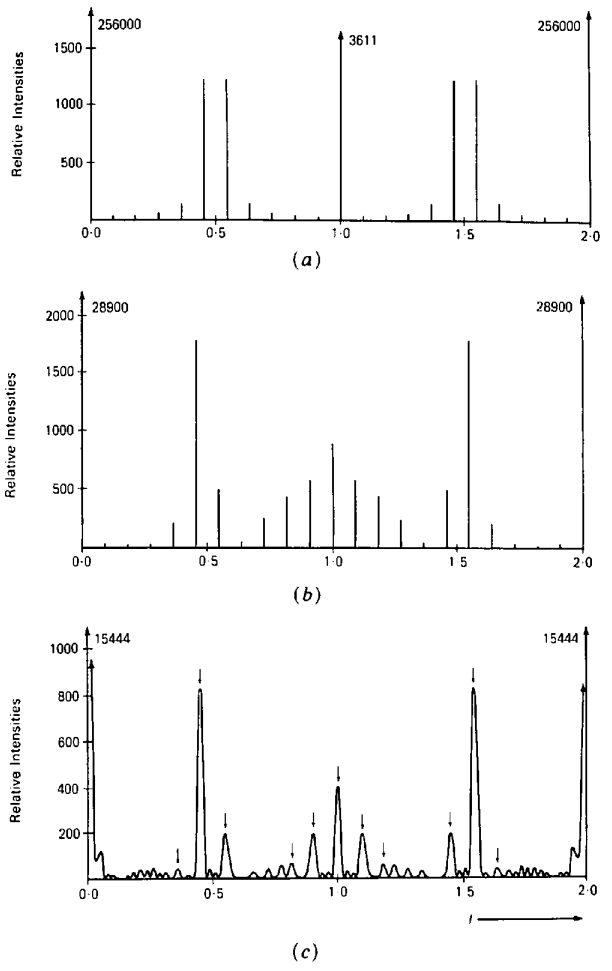

Fig. 13. Calculated diffraction pattern for one-dimensional scattering arrays corresponding to models 1 and 2: (*a*) model 1; (*b*) model 2; (*c*) calculated diffraction pattern for superposed domains of different chain length using model 2.

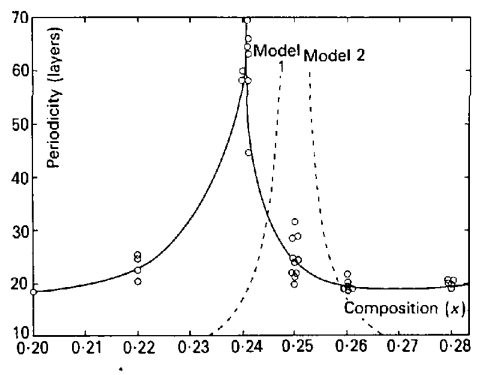

Fig. 14. Periodicity of low-temperature phase as a function of composition and calculated compositions for models 1 and 2.

For the observed range of N, models 1 and 2 result in compositions x as shown in Fig. 14. For $x = 0{\cdot}25$, N in both models goes to infinity and the models become identical. Also plotted in Fig. 14 are experimentally determined chain lengths for different compounds below T_B. A comparison between Figs. 14 and 2 suggests a correlation between the incommensurate lattice period and the transition temperature T_B.

Regardless of the specific arrangement of vacancies the observed changes with a crystal - for instance due to temperature changes - may be understood in terms of vacancy migration. The specific arrangement of the vacancies may be different for different temperatures. At least in one case, namely for $K_{0{\cdot}25}WO_3$, a temperature-related phase change was observed.

The arrangement in symmetrically equivalent channels must be the same or at least strongly correlated since otherwise no incommensurate superlattices would be observed. Perfect ordering within each channel but disorientation of the chains relative to one another would result in diffuse streaks or sheets in the diffraction pattern perpendicular to the direction of the chain. Such diffuse streaks or sheets were occasionally observed. In channel positions that are not equivalent (as indicated by commensurate superlattices) the chains may be translated by one half period.

The complexity of the images as well as of the diffraction patterns suggests that perhaps each single crystal consists of a variety of compositions. Electron-microscope data, which deal with only one relatively small section at a time, would therefore have to be evaluated on a statistical basis.

In spite of a great number of measurements, many questions remain to be answered. But the present data show an interesting correlation between vacancy ordering and electrical transport properties.

The authors wish to thank the HVEM faculty at Argonne National Laboratory, Argonne, IL, for the use of their facility, Dr Charles Allen for taking the crystal image (Fig. 8), Dr Sumio Iijima for thinning two samples and Mr Bret Ripley for numerous tedious measurements of diffraction patterns and other work related to this paper.

References

BANDO, Y. & IIJIMA, S. (1980). *Proceedings of the 38th Annual EMSA Meeting*, edited by G. W. BAILEY, pp. 166-167. Baton Rouge: Claitor.

CALDWELL, L. N., MORRIS, R. C. & MOULTON, W. G. (1981). *Phys. Rev. B*, **23**, 2219-2223.

FERRETTI, A., ROGERS, D. B. & GOODENOUGH, J. B. (1965). *J. Phys. Chem. Solids*, **26**, 2007-2011.
GOODENOUGH, J. B. (1965). *Bull. Soc. Chim. Fr.* **4**, 1200-1201.
MAGNÉLI, A. (1953). *Acta Chem. Scand.* 7, 315-324.
SATO, M., GRIER, B. H, SHIRANE, G. & FUJISHITA, J. (1982). *Phys. Rev. B*, **25**, 501-503.
SIENKO, M. J. (1963). *Adv. Chem.* **39**, 224-245.
SKOKAN, M. R., MOULTON, W. G. & MORRIS, R. C. (1979). *Phys. Rev. B*, **20**, 3670-3677.
STANLEY, R., MORRIS, R. C. & MOULTON, W. G. (1978). *Solid State Commun.* **27**, 1277-1280.
STANLEY, R. K., MORRIS, R. C. & MOULTON, W. G. (1979). *Phys. Rev. B*, **20**, 1903-1914.

Acta Cryst. (1985). B**41**, 21-26

Crystal Structure of $KLiSO_4$ as a Function of Temperature

BY HEINZ SCHULZ, UDO ZUCKER* AND ROGER FRECH†

Max-Planck-Institut für Festkörperforschung, Heisenbergstrasse 1, *D*-7000 *Stuttgart* 80, *Federal Republic of Germany*

(*Received* 3 *April* 1984; *accepted* 23 *August* 1984)

Abstract

A crystal structure investigation focused on the thermal motion of O and Li and based on single-crystal X-ray diffraction data (Mo $K\alpha$) has been carried out at 293, 398 and 568 K in space group $P6_3$ with the assumption of complete atomic order. Anharmonic temperature factors based on the Gram-Charlier expansion have been refined up to the third order for O and Li with about 600 observed F_o values (R_w = 0·017-0·024). Probability densities (O, Li) and one-particle potentials have been calculated from the coefficients of the temperature factors. These allow the following conclusions: both oxygens show large and strongly anharmonic thermal motion as well as static disorder; the oxygens on the threefold axes [O(1)] vibrate mainly perpendicular to **c** with a pronounced threefold symmetry; O(2) atoms exhibit their main vibrations parallel to **c**. The thermal vibrations can be explained by coupled rotational vibrations of the oxygens around the S atoms. The Li atoms develop a strong anharmonic thermal motion above 400 K with a pronounced threefold symmetry.

Introduction

$KLiSO_4$ undergoes several phase transitions; those at approximately 180, 700 and 950 K may be considered as main transitions.

The phase transition at 180 K has been investigated by Raman scattering (Bansal, Deb, Roy & Sahni, 1980), pyro- and dielectric studies (Breczewski, Krajewski & Mróz, 1981; Madhu & Narayanan, 1981), piezoelectric studies (Mróz, Krajewski, Breczewski, Chomka & Sematowicz, 1982), X-ray diffraction (Tomaszewski & Lukaszewicz, 1982) and NMR studies (Meng-Quingan & Cao-Quijuan, 1982). An orthorhombic structure model has been proposed for the low-temperature phase (≤ 180 K) by Tomaszewski & Lukaszewicz (1982).

An intermediate phase has been reported in a temperature range of about 250-180 K. Further conclusions on this phase are contradictory. Bansal, Deb, Roy & Sahni (1980) propose from Raman-scattering data a trigonal structure caused by cooperative reorientation of the tetrahedra. For the same phase Tomaszewski & Lukaszewicz (1982) assume a hexagonal structure to explain their X-ray diffraction data. Holuj & Drozdowski (1981) found hints in an EDR study that this phase may have an incommensurate structure.

The phase transition at 700 K was found by several experimental techniques, including double reflection (Blittersdorf, 1929), differential thermal analysis (Lepeshkov, Bodaleva & Kotova, 1961), measurements of thermal-expansion coefficients, DC resistivity, pyroelectric current and dielectric constants (Ando, 1962), X-ray diffraction study (Prasad, Venudhar, Iyengar & Rao, 1978; Fischmeister & Rönnquist, 1960), and Raman scattering (Bansal, Deb, Roy & Sahni, 1981).

The phase transition at 950 K was detected by differential thermal analysis (Lepeshkov *et al.*, 1961). The phases stable up to 946 K and stable above 946 K are reported to show orthorhombic and hexagonal symmetry, respectively (Schroeder, 1975).

The physical properties of $KLiSO_4$ reported in the above-mentioned papers deal with the two phases stable below and above 190 K. The low-temperature phase has been shown to be ferroelastic (Mróz *et al.*,

* Present address: Robert Bosch GmbH, Post Box 50, D-7000 Stuttgart, Federal Republic of Germany.
† Present address: Department of Chemistry, University of Oklahoma, Norman, Oklahoma 73019, USA.

0108-7681/85/010021-06$01.50